Available online at www.sciencedirect.com
ScienceDirect
ELSEVIER
Electronic Notes in Theoretical Computer Science 225 (2009) 255–268
Electronic Notes in Theoretical Computer Science
www.elsevier.com/locate/entcs

Combined Effects of Frequency Quantization and Additive Input Noise in a First-order Digital PLL

Cillian Ó Tuama[1] and James P. Gleeson[2]

Department of Applied Mathematics
University College Cork
Cork, Ireland

Abstract

A recent work by Gardner [1] on the subject of digital phase-locked loops (DPLLs) investigated, via simulation, the characteristics of the phase-jitter caused by frequency quantization in the numerically-controlled oscillator. Further works by Feely, Teplinsky et al [2], [3] used the theory of nonlinear dynamics to provide a complete analytical explanation of this phase-jitter.
This paper examines in detail the case where the input signal is embedded in additive noise, a scenario earlier investigated by Gardner where no satisfactory method of characterising the phase-jitter was found. Here, further numerical results for the 1-D DPLL are presented and it is shown analytically how the DPLL noise-jitter dynamics may be approximated by a noisy circle rotation map for reasonable levels of additive noise. The noise in this case is unique and highly nonlinear in nature and thus not amenable to traditional analysis. By considering the the probability flow over time, a time-dependent difference-delay equation is derived for the probability density function (PDF) of the phase-jitter. It is shown that this PDF reaches a steady-state and that this state is described by a non-local equation. The solutions of this equation are investigated, both numerically and analytically, and used to explain the interaction between the additive and quantization noise that was previously not understood.

Keywords: Nonlinear dynamics, phase jitter, phase-locked loops.

1 Introduction

Phase-locked loops (PLLs) have been widely used for many years as components in electronics, and in communications systems in particular. A PLL is a closed loop consisting of a phase-detector, linear filter, and a voltage-controlled oscilllator (VCO) as shown in Figure 1 and as described and analysed in detail in [4]. When arranged as shown, the feedback signal entering the oscillator acts as an error signal, and drives the phase of the oscillator to match that of the input signal. Because of this property, PLLs are often used to synchronize clock signals across devices as well

[1] Email: cotuama@gofree.indigo.ie
[2] Email: j.gleeson@ucc.ie

doi:10.1016/j.entcs.2008.12.079

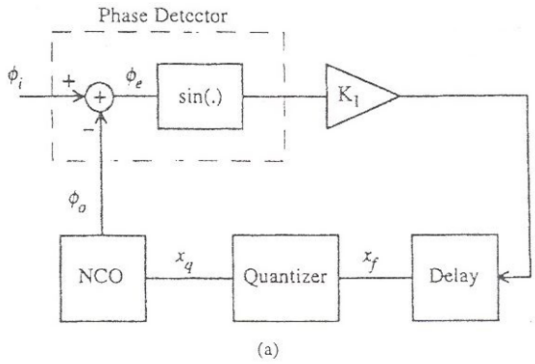

Fig. 1. Block diagram of first-order DPLL from [2]

as to extract carrier signals in communications devices. With some straightforward modifications to the circuit, a PLL can also be used as a frequency multiplier or divider.

Most modern communications systems are digital in nature i.e. rely on discrete-time sampling of the incoming signal, which are then fed into the digital PLL (DPLL). In this case the PLL is simply a logic device, or perhaps even an algorithm operating on a digital computer, operating over discrete time-steps, and with discretized state values at each point in the loop. The VCO becomes a number-controlled oscillator (NCO) where the output frequency is determined by the control word x_q that is presented at the input. Since x_q is quantized i.e. can only take on a finite number of values, the output frequency will also be quantized, and, in general, this will prevent the output signal from matching the input signal exactly. This quantization jitter was examined in great detail in [2], [3].

Gardner [1] also examined numerically the case where the input signal was embedded in additive white Gaussian noise, and attempted to derive some rules of thumb to indicate how this additive noise interacted with the quantization jitter. Though some characterization of the output noise was done, the results obtained were only moderately accurate, and were only valid within certain regimes. No overall understanding of the problem was arrived upon.

This paper examines the effect on the output noise of the interaction between the input noise and the quantization jitter by noting that the DPLL operation in its steady-state is the circle-rotation map, and by considering the novel way that the input noise affects the dynamics of this map. From this, we consider the 'flow' of probability over a single time-step, and derive a difference-delay equation for the PDF of the DPLL phase error. From this we obtain a delay-equation for the steady-state solution and look at some of its properties. In particular, from the PDF we can calculate the variance of the phase error in steady-state, which is the quantity generally of interest, since it represents the magnitude of the output noise.

2 Noise free dynamics

2.1 Preliminaries

Definition 2.1 The class of circle rotation maps on $[0, 2\pi)$ is defined as

$$x(t+1) = (x(t) + 2\pi\gamma) \bmod 2\pi, \text{ for } t = 0, 1, 2, \ldots$$

The circle rotation map is periodic with period q if γ is rational and equal to $\frac{p}{q}$ in its lowest form. Otherwise, as in [2], the mapping is quasi-periodic and is dense in $[0, 2\pi)$.

Definition 2.2 The class of circle rotation maps on $[M, M+S)$ is defined as

$$x(t+1) = \begin{cases} x(t) + \alpha & \text{for } M \le x(t) < M + S - \alpha \\ x(t) + \alpha - S & \text{for } M + S - \alpha \le x(t) < M + S \end{cases} \quad \text{for } t = 0, 1, 2, \ldots$$

This second form of the circle map is equivalent to the first except shifted from $[0, 2\pi)$ to $[M, M+S)$ and is periodic if $\frac{\alpha}{S}$ is rational, and quasi-periodic otherwise.

Theorem 2.3 *For a circle rotation map with parameters (M, S, α) as before, where $\frac{\alpha}{S}$ is rational and equal to $\frac{p}{q}$ in its lowest form, the mean value of the mapping is*

$$(M + \delta) + \frac{(q-1)S}{2q}$$

and the variance is

$$\frac{(q^2-1)S^2}{12q^2}$$

where $\delta \in [0, \frac{1}{q})$ is the minimum value of the mapping on $[M, M+S)$.

Proof. Straightforward once it is noted that the set of values taken on by the mapping over a single period is $\{M+\delta, M+\delta+\frac{S}{q}, M+\delta+\frac{2S}{q}, \ldots, M+\delta+\frac{(q-1)S}{q}\}$, though not necessarily in this order. For example, the mean is then calculated as

$$\frac{1}{q}\sum_{n=0}^{q-1}(M + \delta + \frac{nS}{q})$$

$$= (M + \delta) + \frac{S}{q^2}\sum_{n=1}^{q-1} n$$

$$= (M + \delta) + \frac{(q-1)S}{2q}$$

The variance is calculated in a similar fashion. □

Note that in Theorem 2.3 that as $q \to \infty, \delta \to 0$, the mean $\to (M + \frac{S}{2})$ and the variance $\to \frac{S^2}{12}$ as would be expected for a uniformly distributed quasi-periodic mapping on $[M, M+S)$.

2.2 Circle rotation map and 1-D DPLL

Following [2], we assume a sinusoidal input signal of frequency ν so that its phase, $\phi_i(t)$ in Figure 1, is

$$\phi_i(t) = 2\pi t\nu \bmod 2\pi \tag{1}$$

for $t = 0, 1, 2, \ldots$. The quantizer produces a b-bit quantized version of the loop filter output $x_f(t)$

$$x_q(t) = \frac{1}{2^b}\text{Int}[2^b x_f(t)] \tag{2}$$

where $\text{Int}[x]$ denotes the integer part of x. x_q is used as the input control word for the NCO, whose output frequency is proportional to the input, so that its phase is

$$\phi_o(t) = \phi_o(t-1) + 2\pi x_q(t) \bmod 2\pi \tag{3}$$

Since x_q is quantized, so also are the NCO phase and frequency. This implies that the NCO output signal will, in general, not be able to lock exactly to the input signal, but will instead incur a steady-state phase jitter

$$\phi_e(t) = \phi_i(t) - \phi_o(t) \tag{4}$$

For the first-order loop in Figure 1 the loop filter output x_f is

$$x_f(t) = K_1 \sin(\phi_e(t-1)) \tag{5}$$

Combining equations (1)-(5) we have, finally, as in [2]

$$\Phi(t+1) = \Phi(t) + \frac{2\pi}{2^b}(\mu - \text{Int}[2^b K \sin\Phi(t)]) \text{ for } t = 0, 1, 2, \ldots \tag{6}$$

Here $\Phi(t) = \phi_e(t)$ is the phase error, $\mu = 2^b\nu$, and $K = K_1$ is the loop gain.

Theorem 2.4 *For a sufficiently small input frequency, the steady-state DPLL phase error obeys a circle rotation map.*

Proof. Letting $A = \mu - \text{Int}[2^b K \sin\Phi(t)]$, note that $\Phi(t)$ will continue to increase as long as $A > 0$ and will decrease only when $A < 0$. For $A < 0$ require

$$\text{Int}[2^b K \sin\Phi(t)] \geq \text{Int}[\mu] + 1$$

$$\text{i.e. } 2^b K \sin\Phi(t) \geq \text{Int}[\mu] + 1$$

$$\text{i.e. } \sin\Phi(t) \geq \frac{\text{Int}[\mu]+1}{2^b K}$$

This requires $\text{Int}[\mu] \leq 2^b K - 1$, a limitation on the input frequency, reflecting the fact that, in general, a 1-D PLL can only lock to a finite range of frequencies. So, assuming small initial conditions such that $\text{Int}[2^b K \sin\Phi(0)] = 0$, and that $\Phi(t)$ remains in the range $[0, \frac{\pi}{2}]$, $\Phi(t)$ will continue to increase until $\Phi(t) \geq \arcsin\frac{\text{Int}[\mu]+1}{2^b K}$. Also, if $K < \frac{1}{2\pi\mu}$, then $\text{Int}[2^b K \sin\Phi(t)]$ will never jump by more than 1, so $\Phi(t)$

will increase from its initial value until it enters a regime where it increases only by a fixed step of $\frac{2\pi}{2^b}\text{Frac}[\mu]$, where Frac$[x]$ is the fractional part of x. Finally, when it exceeds $\arcsin\frac{\text{Int}[\mu]+1}{2^bK}$, it will then decrease by a step of $\frac{2\pi}{2^b}$ - $\frac{2\pi}{2^b}\text{Frac}[\mu]$. That is to say, in this region, Φ obeys the mapping

$$\Phi(t+1) = \begin{cases} \Phi(t) + \frac{2\pi}{2^b}\text{Frac}[\mu] & \text{for } \Phi(t) < \arcsin\frac{\text{Int}[\mu]+1}{2^bK} \\ \Phi(t) + \frac{2\pi}{2^b}\text{Frac}[\mu] - \frac{2\pi}{2^b} & \text{for } \Phi(t) \geq \arcsin\frac{\text{Int}[\mu]+1}{2^bK} \end{cases} \quad \text{for } t = 0, 1, 2, \ldots$$

This is a circle rotation map with $M = \arcsin\frac{\text{Int}[\mu]+1}{2^bK} + \frac{2\pi}{2^b}\text{Frac}[\mu]$, $S = \frac{2\pi}{2^b}$, and $\alpha = \frac{2\pi}{2^b}\text{Frac}[\mu]$.

□

It should be noted from Theorem 2.4 above that the nature of the motion (periodic, quasi-periodic) depends only on $\frac{\alpha}{S} = \text{Frac}[\mu] = \text{Frac}[2^b\nu]$. Therefore, if the level of quantization, b, is changed and the input frequency altered to compensate such that μ remains constant, only the scale (S) and base (M) of the mapping changes. Theorem 2.3 may be used to calculate the variance of the mapping when μ is known, or to obtain bounds on the variance when it is not.

3 1-D DPLL and noise

We are interested in the behaviour of the DPLL when noise is added to the input signal, since this is what is encountered by designers, and, as mentioned in [1], there is no clear understanding of this problem. As mentioned in [5], it is equivalent to model the noise as being added after the phase detector. This makes the simulation of the problem somewhat easier in that the noise enters equation 6 as an additional delayed input to the quantizer Int[...]. Therefore, the numerical results in the following section involve simulating the difference equation 8 below, allowing $\Phi(t)$ reach steady state, when at time step the noise sample $N(t)$ is drawn randomly from a uniform density with bounds determined by the input noise variance.

3.1 Numerical results

The main numerical results of the 1-D PLL are shown in Figure 2. The response of the variance of the output jitter to input noise variance is displayed for various DPLL quantization levels. Three distinct regions can clearly be identified. The first is where the additive noise has little or no effect, and the output variance can easily be calculated or bounded using Theorem 2.3. Unsurprisingly, the DPLLs with lower quantization values have a higher noise-free variance, but are also less sensitive to the input noise i.e. it requires a higher level of input noise to effect the output. The PDF of the output jitter in this region is dependent on whether the corresponding circle rotation map is periodic or quasi-periodic, which in turn is determined by Frac$[\mu]$.

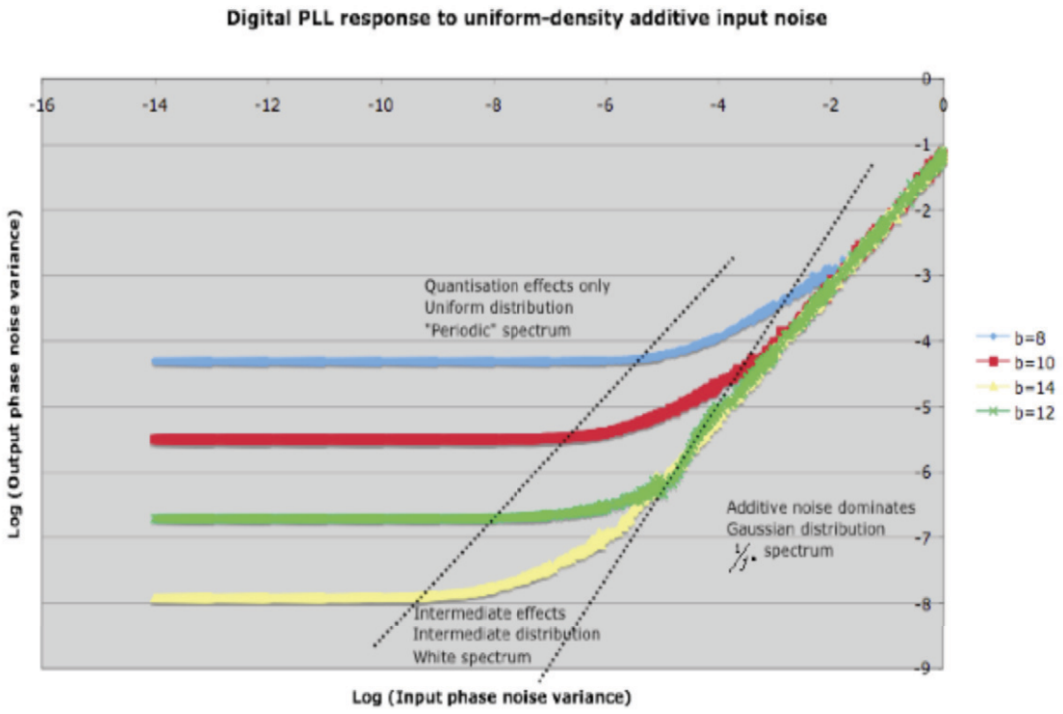

Fig. 2. Variance of DPLL output jitter as a function of input noise variance

The second, intermediate, region is where the additive noise starts to have an effect, but there is also still a significant dependency on the quantization level, demonstrating that the additive noise and inherent jitter are interacting in some way. The region encompasses several orders of magnitude on both the input and output variance axes, and there are points where, for example, the output variance has risen to over an order of magnitude above the noise-free level, but quantization still has an significant effect. Given this, an understanding of the behaviour in this region should be of interest to PLL designers. In addition it was noted that the PDF of the output jitter becomes closer to Gaussian as this intermediate region is traversed.

The final region is where the output variance is independent of quantization, and the graph of the output variance is a line of slope 1. This, as expected, and as noted in [1], is exactly the response of a linear, analogue PLL. The PDF of the output in this region is close to Gaussian.

It should be noted that the parameter μ (and ν) has little effect on these plots. The transition to the intermediate region may occur slightly differently when viewed on a linear, rather than logarithmic, scale, but the overall behaviour is essentially the same.

In Figure 3, the response of the corresponding circle rotation maps to the same input noise levels are shown. In general they track the DPLL plots until the noise levels become large. Two characteristics are then noticeable: once they start deviating from the DPLL plots, each circle map plot continues with in a straight line

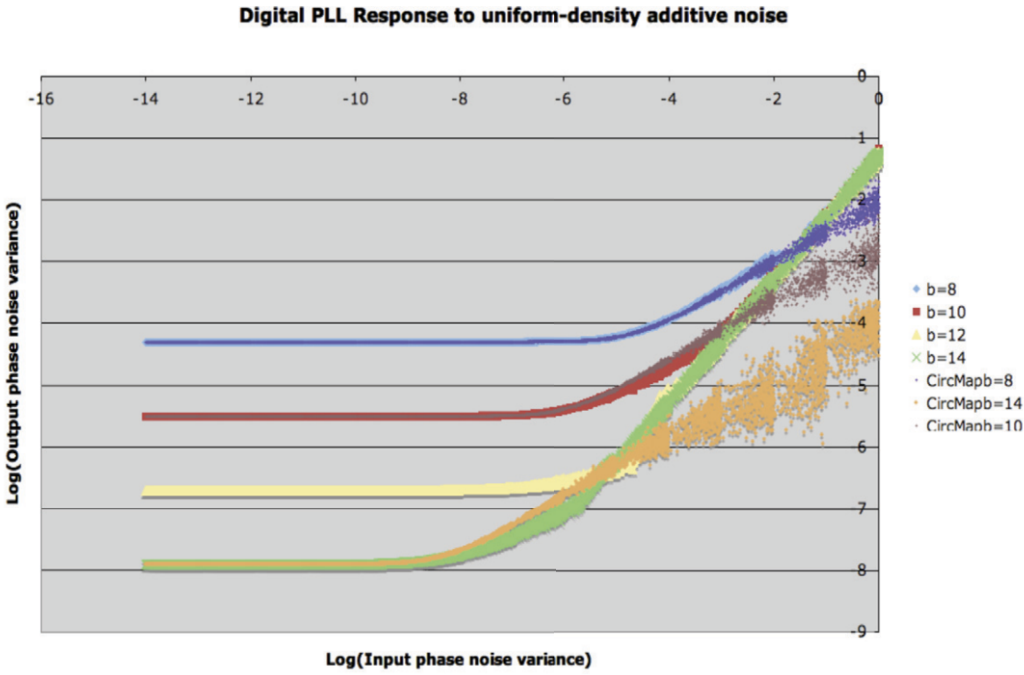

Fig. 3. Variance of DPLL output jitter as a function of input noise variance, with corresponding circle rotation maps shown

with slope of approximately $\frac{1}{2}$, and also the response becomes unstable as the measured output variance fluctuates wildly. The latter is an artefact of the simulation technique used. In any event, this is of little importance as this behaviour is evident only in the region where each DPLL is responding like an analogue PLL. It should be clear from the plot that the regime where the circle map variance begins increasing with slope $\frac{1}{2}$ corresponds to the intermediate region in the DPLL response, so the behaviour of the DPLL in this region may be explained by an analysis of the large-noise response of the circle map.

3.2 Analysis as circle rotation map

An alternative way of writing the circle rotation map in Definition 2.2 is as follows

$$x(t+1) = x(t) + \alpha + Q(x(t))S, \text{ for } t = 0, 1, 2, \ldots, \text{ where}$$

$$Q(x) = \begin{cases} -1 \text{ if } x \geq M + S - \alpha \\ 0 \quad \text{if } x < M + S + \alpha \end{cases} \tag{7}$$

In the case where noise is added to the input signal to the DPLL, the equation

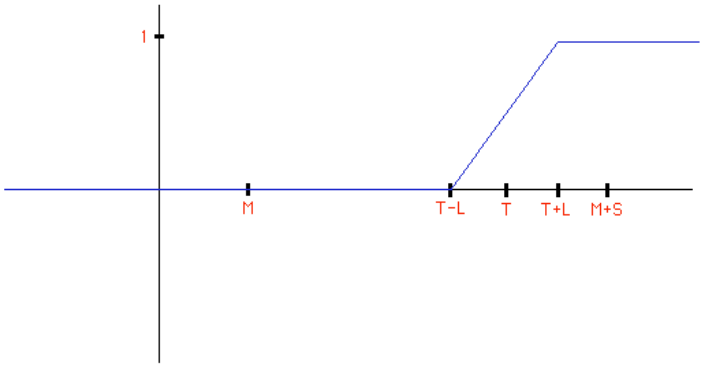

Fig. 4. Function $f(x)$ in case where additive noise is uniformly distributed in $[-L, L]$

governing the behaviour of the output phase error is as follows

$$\Phi(t+1) = \Phi(t) + \frac{2\pi}{2^b}\{\mu - \mathrm{Int}[2^b K(\sin\Phi(t) + N(t))]\} \tag{8}$$

Here $N(t)$ is the noise sample added after the phase-detector at time-step t, and, again, is statistically equivalent to adding it to the input signal.

Remark 3.1 For large noise i.e. $N(t) \gg \sin\Phi(t)$ and $N(t) \gg \frac{\nu}{K}$, (8) can be approximated by

$$\Phi(t+1) = \Phi(t) - 2\pi K N(t) \tag{9}$$

In this case $\phi(t)$ obeys a random walk and thus is non-stationary so no steady-state variance exists. This paper considers only cases where steady-state solutions occur.

The addition of the random noise sample in (8) will sometimes cause the quantizer (Int[...]) to output a value other than what it would have done in the noise-free case. The DPLL can therefore be modeled by a noisy circle rotation map as follows

$$x(t+1) = x(t) + \alpha + Q(x(t))S, \text{ for } t = 0, 1, 2, \ldots, \text{ where}$$

$$Q(x) = \begin{cases} -1 \text{ with probability } f(x) \\ 0 \quad \text{with probability } 1 - f(x) \end{cases} \tag{10}$$

In the above, the function $f(x)$ represents the the PDF, $P(y)$, of the noise, $N(t)$, as follows

$$f(x) = C(x - T), \text{ where } T = (M + S - \alpha), \text{ and } C(x) = \int_{-\infty}^{x} P(y)dy$$

$f(x)$ is shown in Figure 4 for the case where $N(t)$ is uniformly distributed in $[-L, L]$. The variance, σ_N^2, is $\frac{L^2}{3}$ in this case.

We are interested in finding the statistics of $x(t)$, given those of $N(t)$, and its variance in particular. Therefore it makes sense to define the time-dependent PDF of $x(t)$ as $p(x, t)$, where $x \in \mathbb{R}$, $t = 0, 1, 2, \ldots$

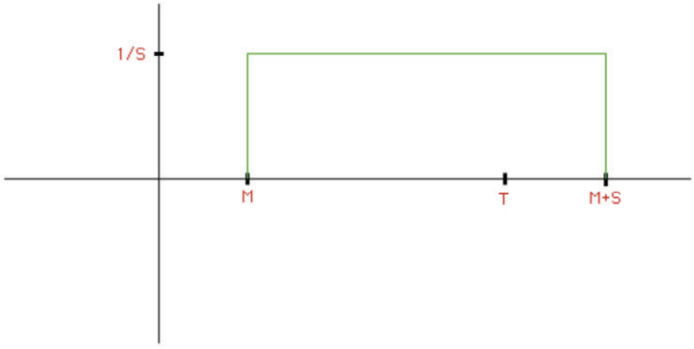

Fig. 5. Initial distribution $p(x,0)$ in case of quasi-periodic circle rotation map

Theorem 3.2 *For the noisy circle rotation map as defined in (10), the PDF, $p(x,t)$, of $x(t)$ obeys the following equation*

$$p(x,t) = p(x-\alpha, t-1)[1-f(x-\alpha)] + p(x-\alpha+S, t-1)f(x-\alpha+S) \qquad (11)$$

Proof. Consider how $p(x,t)$ changes over a single timestep. It is increased by a flow from $x-\alpha$ i.e. by an amount $p(x-\alpha,t-1)[1-f(x-\alpha)]$. It is also increased by a flow from $x-\alpha+S$ i.e. by $p(x-\alpha+S,t-1)f(x-\alpha+S)$. Finally, $p(x,t)$ is decreased by the flow from x (no matter whether the flow is to $x+\alpha$ or $x+\alpha-s$) i.e. by $p(x,t-1)$. Combining, we obtain

$$p(x,t)-p(x,t-1) = p(x-\alpha,t-1)[1-f(x-\alpha)]+p(x-\alpha+S,t-1)f(x-\alpha+S)-p(x,t-1)$$

From this, the result follows. □

This result may be used to simulate the behaviour of the PDF of x by evolving it over time from an initial condition $p(x,0)$. For example, in the case of an irrational Frac$[\mu]$, the mapping is quasi-periodic, and the ensemble will initially be uniformly distributed in $[M, M+S)$ as shown in Figure 5.

In the case of the circle map with the range of parameters used in Figure 3, and $f(x)$ as in Figure 4, it was verified numerically that, starting from a uniform distribution on $[M, M+S)$, the PDF $p(x,t)$ quickly reached a steady state, and that for larger levels of input noise the PDF was approximately Gaussian with a kurtosis close to 3, though the tails of the distribution quickly went to zero.

If the PDF in (11) does reach a steady-state $P_\infty(x)$ it is described by

$$P_\infty(x)f(x) = P_\infty(x+\alpha-S) - P_\infty(x-S)[1-f(x-S)] \qquad (12)$$

Theorem 3.3 *For the steady-state distribution $P_\infty(x)$ given in (12), $f(x)$ as in Figure 4, and initial distribution $P(x,0)$ that is zero outside the range $(M-L, M+S+L)$ (e.g. that given in Figure 5), $P_\infty(x)$ is identically zero outside a region of size $(2L+S)$ that contains $x=T$.*

Proof. For $x \le T-L+\alpha-S = M-L$ we have $f(x-\alpha+S)=0$ and $f(x-\alpha)=0$ from Figure 4. Then (11) becomes $p(x,t) = p(x-\alpha,t-1)$ and hence $p(x,t) = p(x-t\alpha,0)$.

Since $x \leq M - L$, $x - t\alpha \leq M - L$ also, so $p(x - t\alpha, 0) = 0$ from Figure 5. Hence $p(x,t) = 0$.
Similarly, for $x \geq T+L+\alpha = M+S+L$ we have $f(x-\alpha) = 1$ and $f(x-\alpha+S) = 1$, so (11) becomes $p(x,t) = p(x+S-\alpha, t-1)$ and hence $p(x,t) = p(x+t(S-\alpha), 0)$. Since $x \geq M+S+L$ and $(S-\alpha) \geq 0$, $x + t(S-\alpha) \geq M+S+L$ also, so $p(x+t(S-\alpha), 0) = 0$ from Figure 5. Hence $p(x,t) = 0$.
Therefore $\forall t$, $p(x,t) = 0$ for $x \leq M - L$ and $x \geq M+S+L$. The same is true of $P_\infty(x)$ if this steady-state solution exists. Clearly, the only region where $P_\infty(x)$ can be non-zero is in $(M-L, M+S+L)$, a region of size $2L+S$ containing $T = M+S-\alpha$. □

Theorem 3.4 *For the steady-state distribution $P_\infty(x)$ given in (12), $f(x)$ as in Figure 4, and in the special case $S = 2\alpha$, $P_\infty(x)$ is approximately Gaussian with a variance of $\frac{1}{4}SL$.*

Proof. (12) becomes

$$P_\infty(x)f(x) = P_\infty(x-\alpha) - P_\infty(x-2\alpha)[1 - f(x-2\alpha)] \tag{13}$$

Using the change of variable $y = x - \alpha$, get

$$P_\infty(y+\alpha)f(y+\alpha) = P_\infty(y) - P_\infty(y-\alpha)[1 - f(y-\alpha)] \tag{14}$$

Using a Taylor expansion $P_\infty(y+\alpha) = P_\infty(y) + \alpha P'_\infty(y) + \frac{\alpha^2}{2}P''_\infty(y) + \ldots$, similarly for $P_\infty(y-\alpha)$, $f(x+\alpha)$, and $f(x-\alpha)$, and neglecting higher-order terms, get

$$2P_\infty(y)f'(y) + (2f(y)-1)P'_\infty(y) + \frac{\alpha}{2}P''_\infty(y) = 0 \tag{15}$$

That is

$$\frac{d}{dy}[(2f(y)-1)P_\infty(y)] + \frac{\alpha}{2}P''_\infty(y) = 0 \tag{16}$$

Now substituting for linear $f(y)$, $2f(y) - 1 = \frac{y-T}{L}$, get

$$\frac{d}{dy}[(\frac{y-T}{L})P_\infty(y)] + \frac{\alpha}{2}P''_\infty(y) = 0 \tag{17}$$

Integrating, and demanding $P_\infty(y)$ and $P'_\infty(y) \to 0$ as $y \to \infty$, obtain

$$(\frac{y-T}{L})P_\infty(y) + \frac{\alpha}{2}P'_\infty(y) = 0 \tag{18}$$

That is

$$\frac{P'_\infty(y)}{P_\infty(y)} = \frac{-2(y-T)}{\alpha L} \tag{19}$$

Integrating again, get, for some constant C_1

$$P'_\infty(y) = C_1 \exp\left[\frac{-1}{\alpha L}(y^2 - 2Ty)\right] \tag{20}$$

Completing square, letting $C = C_1 \exp\left[\frac{1}{\alpha L}T^2\right]$, have finally

$$P'_\infty(y) = C \exp\left[\frac{-1}{\alpha L}(y-T)^2\right] \tag{21}$$

This is a Gaussian of mean T and variance $\frac{1}{2}\alpha L = \frac{1}{4}SL$. □

Remark 3.5 By substituting for L, the variance can also be written as

$$\frac{1}{4}S\left(3\sigma_N^2\right)^{\frac{1}{2}}$$

Here σ_N^2 is the variance of the additive noise and this verifies analytically the numerical results for the circle map shown earlier in Figure 3, at least for the special case $S = 2\alpha$.

To simulate (12) on a computer the space variable may be discretized by taking a fixed mesh size δ, and letting $x = m\delta$, $S = N\delta$, and w.l.og. $\alpha = \delta$ (mesh normalized to α, and $S = N\alpha$). Then, writing $P_\infty(a\delta)$ and $f(a\delta)$ as p_a and f_a respectively, (12) can be written in discrete form

$$p_m f_m = p_{m+1-N} - p_{m-N}(1 - f_{m-N}) \tag{22}$$

Numerical simulation of (22) verified the Gaussian-type distribution obtained in the steady-state of time-dependent (11). Again, outside of a certain range about T, the distribution is identically zero. Indeed this can easily be proved using (11).

Some further properties of the solution $P_\infty(x)$ can be seen by an examination of (22). For the special case $N = 2$, as in Theorem 3.4, this becomes

$$p_m f_m = p_{m-1} - p_{m-2}(1 - f_{m-2}) \tag{23}$$

As before let $f(x)$ be as shown in Figure 6 on the discrete x-axis i.e. identically zero for $x \le A$, identically 1 for $x \ge B$ and linear in $[A, B]$. Here $T - L = A\delta$ and $T + L = B\delta$ and $f(x)$ at $x = m\delta$, $m \in \mathbb{Z}$, is denoted f_m.

Theorem 3.6 *For $f(x)$ given in Figure 6 and p_m satisfying (23) the solution is given as*

$$p_m = \begin{cases} 0 & \text{for } m < A \\ R_{m-A}/\delta & \text{for } A \le m \le B \\ 0 & \text{for } m > B \end{cases} \tag{24}$$

where R_i is the binomial coefficient $\binom{\tilde{N}}{i} q^i (1-q)^{\tilde{N}-i}$, for $q = \frac{1}{2}$ and $\tilde{N} = B - A = \frac{2L}{\delta}$.

Proof. For $m \le A$ (23) becomes $p_{m-1} = p_{m-2}$, since $f_m = f_{m-2} = 0$. From Theorem 3.3 the continuous PDF, $P_\infty(x)$, is zero outside a region centred around $x = T$ so we have $p_m = 0$ as $m \to -\infty$. Hence $p_m = 0$ for $m < A$. Similarly, for $m \ge B + 2$ (23) is $p_m = p_{m-1}$, since $f_m = f_{m-2} = 1$, and so $p_m = 0$ for $m > B$.

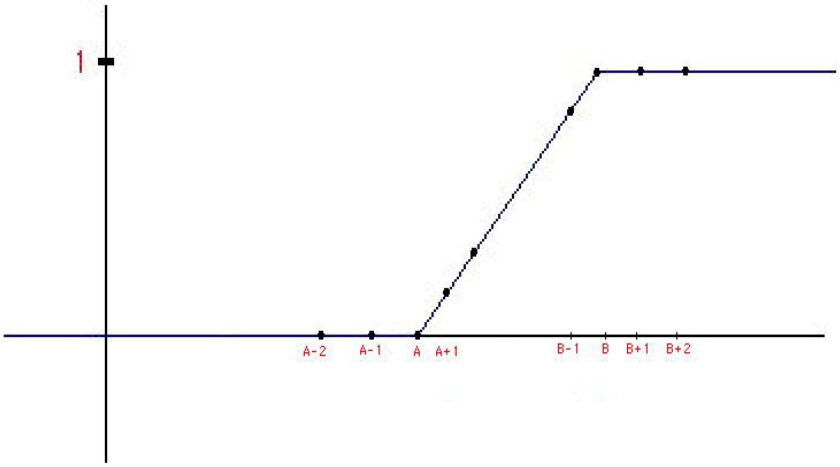

Fig. 6. $f(x)$ from Figure 4 represented on discrete grid

Next, note that $R_{i-1} = \binom{\tilde{N}}{i-1} q^{i-1}(1-q)^{\tilde{N}-i+1} = \frac{\tilde{N}!}{(i-1)!(\tilde{N}-i+1)!} q^{i-1}(1-q)^{\tilde{N}-i+1}$ and $R_i = \frac{\tilde{N}!}{i!(\tilde{N}-i)!} q^i (1-q)^{\tilde{N}-i}$. From this follows the recurrence relation, for $i > 0$

$$R_i = \left(\frac{q}{1-q}\right)\left(\frac{\tilde{N}-i+1}{i}\right) R_{i-1} \tag{25}$$

In the case where $q = \frac{1}{2}$ this becomes

$$R_i = \left(\frac{\tilde{N}-i+1}{i}\right) R_{i-1} \tag{26}$$

Rearranging, and back-substituting for R_{i-1} have, for $i > 1$

$$R_i = \left(\frac{\tilde{N}}{i}\right) R_{i-1} - \left(\frac{\tilde{N}-i+2}{i}\right) R_{i-2} \tag{27}$$

Now for $i > A$, $f_i \neq 0$ and (23) can be rewritten as

$$p_i = \frac{p_{i-1}}{f_i} - \frac{p_{i-2}(1-f_{i-2})}{f_i} \tag{28}$$

For $f(x)$ shown in Figure 6 have $f_{i+A} = \frac{i}{\tilde{N}}$ and inserting in (28) we obtain

$$p_{i+A} = \left(\frac{\tilde{N}}{i}\right) p_{i+A-1} - \left(\frac{\tilde{N}-i+2}{i}\right) p_{i+A-2} \tag{29}$$

It should be clear that p_{i+A} satisfies the same recurrence relation as (27) for R_i for $i > 1$. Additionally, $R_0 = \left(\frac{1}{2}\right)^{\tilde{N}}$ and $R_1 = \tilde{N}\left(\frac{1}{2}\right)^{\tilde{N}}$, so $R_1 = \tilde{N} R_0$. Inserting

$m = A + 1$ in (23) we get $p_{A+1} = \tilde{N} p_A$, since $p_{A-1} = 0$ and $f_{A+1} = \frac{1}{\tilde{N}}$. Therefore p_{i+A} and R_i satisfy the same recurrence relations (27), (29) for $i > 0$.
p_A is indeterminate from (23), but since the the values of the p_i represent the steady-state PDF of x we have $\sum_{i=A}^{A+\tilde{N}} p_i = \frac{1}{\delta}$. Also, the R_i are just the binomial coefficients, $\sum_{i=0}^{\tilde{N}} R_i = (q + (1-q))^{\tilde{N}} = 1$.
Since the recurrence relation (25) for the R_i is linear, the value of p_A can be chosen such that $\sum_{i=A}^{A+\tilde{N}} p_i$ is any multiple of $\sum_{i=0}^{\tilde{N}} R_i$. Hence we choose $p_A = R_0/\delta$ so that $p_{A+i} = R_i/\delta$,$\forall i$, and $\sum_{i=A}^{A+\tilde{N}} p_i = \frac{1}{\delta} \sum_{i=0}^{\tilde{N}} R_i$. This proves relation (24). □

Remark 3.7 For fixed δ we have $\tilde{N} = \frac{2L}{\delta}$, so the large noise case, $L \to \infty$, corresponds to $\tilde{N} \to \infty$. Given that the binomial coefficients R_i, $i = 0, \ldots, \tilde{N}$, given in (26) tend towards the discrete samples of the Gaussian as $\tilde{N} \to \infty$, Theorem 3.6 has effectively proved that the steady-state phase error PDF becomes Gaussian as the additive noise, $N(t)$, becomes large.

Remark 3.8 Note that with the parameters chosen in Theorem 3.6, $\alpha = \delta$, $S = 2\delta$, $L = \frac{\tilde{N}}{2}\delta$, corresponds to the case where the bounds of the original circle map are vanishingly small as compared to the grid size. Only in the large-noise limit does the observation made in Remark 3.7 apply. In addition, the circle map is of the special type $\alpha = \frac{S}{2}$. However, from the numerics it was found that the overall output variance response didn't depend significantly on the dynamics of the original circle map.

Remark 3.9 The mean and variance of the steady-state PDF (24) can readily be calculated. The mean is

$$\sum_{m=0}^{\tilde{N}} \delta(m + A)(\frac{1}{\delta}) R_m \delta \tag{30}$$

$$= (A \sum_{m=0}^{\tilde{N}} R_m + \sum_{m=0}^{\tilde{N}} m R_m)\delta \tag{31}$$

Using a result from [6] this is simply

$$(A + q\tilde{N})\delta \tag{32}$$

For $q = 1/2$ this is $(A + \tilde{N}/2)\delta = T$. That is, the steady-state noisy circle map PDF is centred at $x = T$ as expected.
The variance is calculated similarly. First of all, we have

$$\sum_{m=0}^{\tilde{N}} \delta^2 (m + A)^2 (\frac{1}{\delta}) R_m \delta = \delta^2 (\sum_{m=0}^{\tilde{N}} m^2 R_m + 2A \sum_{m=0}^{\tilde{N}} m R_m + A^2 \sum_{m=0}^{\tilde{N}} R_m) \tag{33}$$

Again, using results from [6] this is

$$\delta^2 \{(\tilde{N}q)^2 + \tilde{N}q(1-q) + 2Aq\tilde{N} + A^2\} \tag{34}$$

The variance is then, subtracting off the square of the mean (32),

$$\delta^2 \tilde{N} q(1-q) \tag{35}$$

Substituting back the variables for the continuous steady-state PDF and setting $q = 1/2$ this is

$$\frac{1}{4}\delta^2 \tilde{N} = \frac{1}{4} SL \tag{36}$$

This agrees with the result found earlier in Theorem 3.4.

4 Conclusion

It has been shown that under certain conditions, the steady-state dynamics of the 1-D DPLL are identical to the circle rotation-map. This map was introduced and some of its properties examined, in particular its noise-free variance and how this can be used to predict the phase-jitter variance of the DPLL output due to quantization alone. In addition it was illustrated how additive input noise in the DPLL case corresponds to a unique form of quantization noise in the case of the circle map. An equation for the time-dependent PDF of the phase jitter was obtained, and, using this equation, bounds for the phase jitter were found. An analysis of both the continuous and discrete versions of the equation for the steady-state PDF yielded expressions for the case where $\alpha = \frac{S}{2}$. With a further examination of the steady-state PDF it should be possible to derive an expression for the variance of the circle map in the more general large-noise case for the circle map, thus characterising the intermediate regime response of the DPLL.

References

[1] Gardner, F. M.,*Frequency granularity in digital phase-locked loops*, IEEE Trans. Commun., **44** (1996), 749758.

[2] Feely, O., Rogers, A., and Teplinsky, A., *Phase-jitter dynamics of digital phaselocked loops*, IEEE Trans. Circuits and Systems, Part I: Fundamental Theory and Applications, **46** (1999), 545-558.

[3] Feely, O., and Teplinsky, A., *Phase-jitter dynamics of digital phase-locked loops: Part II*, IEEE Trans. Circuits and Systems, Part I: Fundamental Theory and Applications., **47** (2000), 458-473.

[4] Viterbi, A. J., "Principles of Coherent Communication", New York: McGraw-Hill, 1966

[5] Gardner, F. M., "Phaselock techniques", 2nd ed. New York: Wiley, 1979, ch. 3.

[6] Reichl, L. E., "A Modern Course in Statistical Physics", 1st ed. University of Texas Press, 1984, ch. 5.